NANO LETTERS

pubs.acs.org/NanoLett

Letter

Elastocaloric Effect in Graphene Kirigami

Luiz A. Ribeiro Junior, Marcelo L. Pereira Junior, and Alexandre F. Fonseca*

Cite This: *Nano Lett.* 2023, 23, 8801−8807

Read Online

ACCESS | Metrics & More | Article Recommendations | Supporting Information

ABSTRACT: Kirigami, a traditional Japanese art of paper cutting, has recently been explored for its elastocaloric effect (ECE) in kirigami-based materials (KMs), where an applied strain induces temperature changes. Importantly, the feasibility of a nanoscale graphene kirigami monolayer was experimentally demonstrated. Here, we investigate the ECE in GK representing the thinnest possible KM to better understand this phenomenon. Through molecular dynamics simulations, we analyze the temperature change and coefficient of performance (COP) of GK. Our findings reveal that while GKs lack the intricate temperature changes observed in macroscopic KMs, they exhibit a substantial temperature change of approximately 9.32 K (23 times higher than that of macroscopic KMs, which is about 0.4 K) for heating and −3.50 K for cooling. Furthermore, they demonstrate reasonable COP values of approximately 1.57 and 0.62, respectively. It is noteworthy that the one-atom-thick graphene configuration prevents the occurrence of the complex temperature distribution observed in macroscopic KMs.

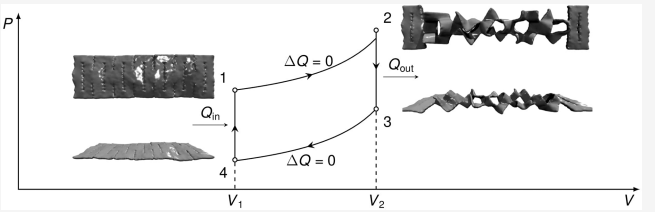

KEYWORDS: *Graphene Kirigami, Elastocaloric Effect, Coefficient of Performance, Molecular Dynamics*

Graphene is a two-dimensional allotrope of carbon atoms arranged in a hexagonal lattice.[1] It was first isolated in 2004 using the mechanical exfoliation technique.[2] Graphene's exceptional combination of mechanical,[3] electronic,[4] thermal,[5,6] and optical properties[7] has made it one of the most extensively studied systems in materials science, with vast potential for use in various applications such as flat electronics,[8] energy storage,[9] and biomedical engineering.[10] However, incorporating graphene into flexible devices poses challenges because of its intrinsically high stiffness, which makes it difficult to bend or stretch. In addition, graphene is brittle, with only a few percent of tensile fracture strains.[11]

Graphene kirigami (GK) is a cutting-edge technique miming the ancient Japanese art of paper-cutting to manipulate graphene.[12] By introducing intricate patterns and tailored structures, GK overcomes the low stretchability barrier of graphene, resulting in unique mechanical properties.[13,14]

Compared to a regular graphene sheet, GK nanostructures exhibit significantly improved reversible stretchability, achieved through multidimensional deformation capabilities enabled by nanoscale kirigami architectures.[15] GK's in-plane stretching and out-of-plane deformation allow for increased flexibility.[15] It is worth noting that GK demonstrates good thermal stability, remaining intact until it reaches a critical temperature of 1600 K,[16] significantly lower than the melting point of graphene, which is approximately 5000 K.[17] With flexible devices being the mainstream trend in modern optoelectronics, kirigami-like materials have become ideal candidates for developing novel applications.

The fabrication of GK structures has yielded remarkable success.[12,16,18−25] Initial work by Blees and colleagues demonstrated the feasibility of GKs, showcasing robust microscale structures with adjustable mechanical properties in graphene.[12] Another experimental study highlighted the strain-insensitive electrical properties of GK-based electrodes, enduring up to 240% tensile strain and various strain states, including stretching, twisting, and shearing.[22]

Density functional theory (DFT) methods are widely used for studying chemical reactions and atom rearrangements due to their ability to accurately describe electronic and lattice structures.[26−29] However, alternative approaches must be considered due to computational limitations in the case of systems consisting of hundreds of electrons or thousands of atoms.[30] Reactive molecular dynamics (MD) has emerged as a suitable approach in these scenarios.[31]

Reactive MD methods explicitly simulate chemical reactions and capture chemistry-based phenomena at the nanoscale with an accuracy comparable to DFT methods.[32−34] Reactive MD can accurately model bond breaking and formation, chemical reactions, and related energy changes using DFT-parametrized force fields.[31] Moreover, reactive MD allows for investigating larger system sizes and longer time scales, providing valuable insights into the behavior of complex systems that would be infeasible using DFT-based methods.[31]

Received: June 16, 2023
Revised: July 18, 2023
Published: July 21, 2023

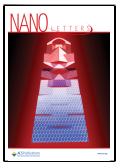

Atomistic MD simulations have extensively investigated GK's stretchability, fracture resistance, and permeability.[13−16,19,20,35−37] Notably, these studies unveiled a noteworthy trend: GK can enhance the fracture strains of graphene by approximately 3-fold compared to standard monolayer graphene. Consequently, the realm of kirigami-inspired nanostructures presents exciting prospects for the fabrication of highly flexible and stretchable devices using graphene[38] and other diverse 2D materials.[39−41]

A temperature change induced by external strain, known as the elastocaloric effect (ECE), has great potential for next-generation thermal management technologies due to its environmental friendliness and economic benefits.[42−44] To make this technology more efficient, efforts have been made to find highly efficient elastocaloric materials.[45−50] In particular, in view of the growing interest in miniaturized refrigeration,[51] at the nanoscale, the study of the ECE in nanostructures has already begun.[52−60]

Recently, a new approach to modulate the elastocaloric temperature change using a kirigami-inspired material was proposed.[61] Results showed that the ultrahigh stretchability of kirigami combined with its lateral flexibility allows for the generation of focused heat absorption and release simultaneously during the same application of tensile or compressive strain, resulting in a versatile local cooling/heating performance.[61] The method can be applied to any elastocaloric material and paves the way for designing versatile solid-state heat pumps for flexible electronics. So far, this phenomenon in kirigami has not been studied on the atomic scale. Moreover, based on the successful synthesis of GKs, a study on the ECE in these materials may open new channels for developing novel thermal management technologies at the nanoscale.

In this study, we employed fully atomistic MD simulations to investigate the ECE in a model GK lattice at the nanoscale. To simulate the ECE in GKs, we modeled a thermal management device under Otto-like thermodynamic cycles, including two adiabatic expansion/contraction processes and two isochoric heat exchange processes. Using our computational protocol, we calculate the GK temperature variations in absorbing and releasing heat and their coefficients of performance.

To investigate the ECE in a model GK lattice at the atomic scale, we used the LAMMPS[62] code with the adaptive intermolecular reactive empirical bond order (AIREBO)[63] potential in reactive MD simulations. This potential accurately addresses carbon-based nanostructures and provides reliable potential energy values to study their mechanical and thermal properties.[17,64−68] Besides, the LAMMPS/AIREBO methodology has been successfully used to describe the ECE in carbon nanomaterials.[52,55,57,58,60] The GK model used in this study is shown in Figure 1 and has the following properties: l_0 = 332 Å, l_1 = 48 Å, l_2 = 4.8 Å, h_0 = 100 Å, h_1 = 68 Å, h_2 = 35 Å, d_f = 19 Å, 12 012 carbon atoms and 1244 hydrogen atoms.

The GK structure was studied under a thermodynamic cycle similar to the Otto cycle, as shown in Figure 2. The cycle consists of two adiabatic expansion/release processes and two volume fixed heat exchange processes with a thermal reservoir at 300 K, in the order 1 → 2 → 3 → 4 → 1. Processes 1 → 2 and 3 → 4 correspond to applying adiabatic tensile strain and release, respectively. Processes 2 → 3 and 4 → 1 represent isochoric heat exchange with a reservoir at 300 K. During the stretching/compression process, the left edge of the kirigami remained fixed, while the right edge was stretched/compressed. In the isochoric heat exchange, both edges remained fixed.

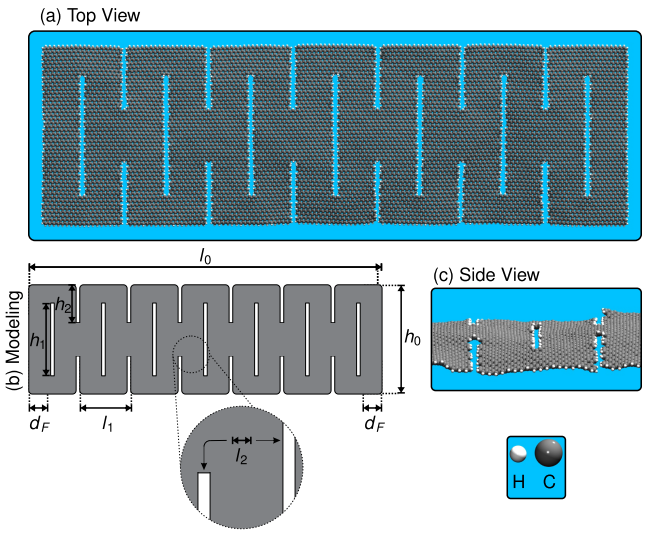

Figure 1. Schematic representation of the model GK lattice studied here. Panels a−c show the GK top view, lattice parameter definitions, and KG side view. In the color scheme, the gray and white spheres represent the carbon and hydrogen atoms, respectively.

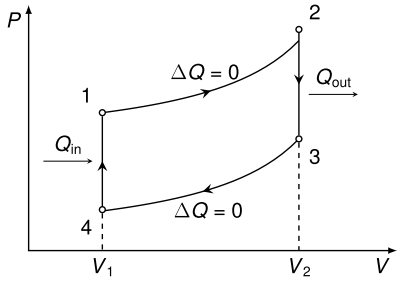

Figure 2. Schematic representation of a p−V-like diagram that illustrates the thermodynamic cycle (1 → 2 → 3 → 4 → 1) used to study the ECE in GK. Processes 1 → 2 and 3 → 4 correspond to the application of adiabatic tensile strain and release, respectively, while processes 2 → 3 and 4 → 1 represent isochoric heat exchange with a reservoir at 300 K.

We minimized the GK structure using force and relative energy tolerances of 1.0 × 10^{-10} eV/Å and 1.0 × 10^{-10}, respectively. The initial GK length (l_0, refer to Figure 1) is 337.20 Å, and its equilibration was then conducted at 300 K, using a constant *NPT* ensemble integration at null pressure using the Nosé−Hoover barostat for 200 ps to ensure no remaining stress.

Here, the thermodynamic cycle was performed as follows: first, we carried out step 1 → 2 (expansion) without a thermostat, subjecting the system to tensile strain from 0% to 30% at a strain rate of 1 × 10^{-4} fs^{-1} during 32 ps, using a time step of 0.02 fs. Second, the step 2 → 3 (isochoric heat exchange) involved a thermal equilibration of 200 ps using the Langevin thermostat and the *NVE* ensemble for a time step of 0.2 fs. The step 3 → 4 (release) was carried out without a thermostat, causing the system to undergo a tensile deformation from 30% to 0% at a strain rate of −1 × 10^{-4} fs^{-1} for 32 ps, again using a time step of 0.02 fs. Finally, step 4 → 1 (isochoric heat exchange) involved another 200 ps of thermal equilibration using the Langevin thermostat and *NVE* ensemble for a time step of 0.2 fs.

https://doi.org/10.1021/acs.nanolett.3c02260
Nano Lett. 2023, 23, 8801−8807

The real variation in the temperature of ECE (ΔT_{REAL}) is obtained by correcting the results of classical MD simulations due to quantum mechanics effects on the specific heat (c) of graphene at 300 K:[52] $\Delta T_{REAL} = (c_{MD}/c_{REAL})\Delta T_{MD}$. Here, "REAL" and "MD" refer to corrected and simulated values, respectively. The $(c_{MD}/c_{REAL}) = 2.53$ factor was obtained using $c_{REAL} = 700\ J{\cdot}kg^{-1}{\cdot}K^{-1}$ from ref 69 and $c_{MD} = 1770\ J{\cdot}kg^{-1}{\cdot}K^{-1}$ from our calculations. c_{MD} was derived from a series of equilibrium simulations for GK subjected to distinct temperature regimes, as discussed later.

We begin our discussion by showing the representative MD snapshots that illustrate the stretching/releasing process of GK (Figure 3). In Figure 3a, we present the top and side views of the KG structure at 0% of strain and equilibrated at 300 K. Even considering the atomic displacements imposed by the temperature effects, one can note that the GK is almost planar, and its pores are of the same size. It is worth mentioning that between 0% and 5% of strain, the GK deformation occurs via stretching of the elastic C−C bond in the direction of the applied strain, similar to the stretching mechanism of graphene nanoribbons.[70] In this low-strain regime, neither out-of-plane flipping nor rotation of the GK pieces is observed.

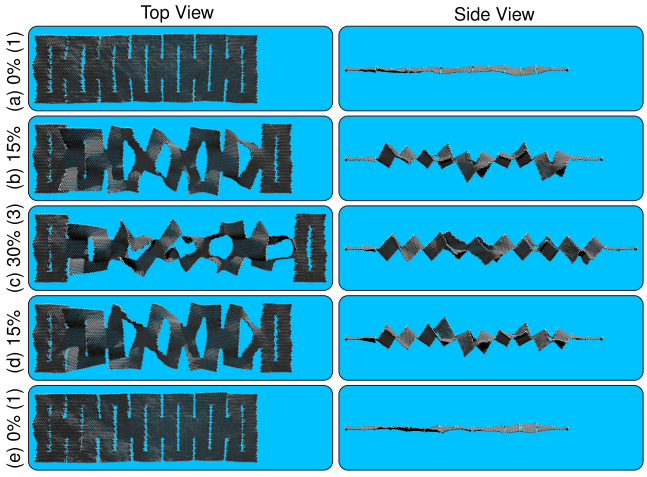

Figure 3. Representative MD snapshots for the GK lattice subjected to the uniaxial strain in the x-direction at 300 K. Panels a−e illustrate the top and side views for the GK structure at 0% strain before stretching, 15% stretching, 30% stretching, 15% releasing, and 0% strain after releasing, respectively. In the color scheme, the gray and white spheres represent the carbon and hydrogen atoms, respectively.

At a strain of 15% (see Figure 3b), noticeable flipping and rotation occurred in certain sections of GK, resulting in varying magnitudes of out-of-plane deflections instead of the anticipated continuous bond stretching in uniformly strained sheets.[71] Unlike pristine graphene nanoribbons that experience failure when reaching a critical strain,[72] these deflections enable the GK monolayer to withstand significantly larger deformations without fracturing.

It is crucial to contrast our findings with the study conducted by Hirai and co-workers,[61] who investigated the electromechanical cooling effect (EMCE) in various macroscopic kirigami materials (KMs). Using sophisticated lock-in thermography techniques, they measured temperature changes across the kirigami surface and discovered that cooling and warming regions coexist within different regions of the structure during the same type of straining (tensile or compressive).

This phenomenon arises from the bending of hole edges within the kirigami plane under tensile strain, inducing both tensile and compressive strains in the outer and inner regions of the bent structure. They also demonstrated that the cooled and warmed regions precisely corresponded to the tensile-strained and compressed parts of the kirigami, respectively. However, we should point out that this effect does not (and cannot) occur in one-atom-thick kirigami.

In our simulations, depicted in Figure 3b−d, the deformation mechanism of GK involves two distinct regions: elastic stretching of C−C bonds (resulting in an ECE increase of temperature) and out-of-plane buckling. Unlike macroscopic kirigami, these buckled regions experienced neither cooling nor warming. This behavior diverges from the EMCE observed in macroscopic KMs. The reason behind this disparity is relatively straightforward. When a thin but macroscopic ribbon flexes, it induces tensile and compressive strains in its outer and inner sections. However, flexing a one-atom-thick nanoribbon, as demonstrated in previous research,[73] does not lead to any bond strain. Therefore, in our case, the out-of-plane deflections did not generate strain in the C−C bonds.

The accumulation of stress in GK is supported by the von Mises stress distribution calculated from an MD study of GK under tension.[15] Consequently, as neither tensile nor compressive strains occur in the out-of-plane deflected regions of GK, there is no heat release or absorption in these areas. In contrast, the heated regions consist of parallel lines of stretched C−C bonds that remain within the GK plane.[15] This stretching mechanism observed in GK opposes the findings of experiments,[61] where stretching elastocaloric materials with a macroscopic kirigami structure resulted in simultaneous heat absorption and release due to nonuniform internal stress generated by uneven strain distribution along the cutting patterns.

Figure 3c shows that the highly stretchable GK pattern, which exhibits no bond breaking or fracture, is achieved at a critical strain of 30%. In this configuration, each GK unit is connected by a small ribbon, allowing the monolayer to be almost foldable. Additionally, a uniform out-of-plane deflection pattern is observed. This configuration limits the interplay between the warming and cooling of GK via ECE temperature variation. Figure 3d and Figure 3e illustrate the GK monolayer configuration during the tensile-releasing mechanism, whose features are similar to those described for Figure 3a and Figure 3b, respectively. We conducted 10 simulations with different seeds for all the thermodynamic cycles; see Supporting Information. For the sake of convenience and to present the qualitative behavior of the entire process, we show the time evolution of the GK temperature under tensile stretching and releasing for just one seed in Figure 4a and Figure 4b, respectively. Figure 4's red and blue lines represent the moving averages for temperature calculated every 100 MD steps.

We obtained the moving averages for all seeds and related average values for ΔT_{MD} and used the $(c_{MD}/c_{REAL}) = 2.53$ factor to find $\Delta T_{REAL} \simeq 9.32$ K during the $1 \rightarrow 2$ tensile stretching process and $\Delta T_{REAL} \simeq -3.50$ K for the $3 \rightarrow 4$ releasing process. The smoothed curves indicate that the GK temperature has an almost linear relationship with time. Additionally, it can be inferred from Figure 4 that the ECE in GK is more significant during heating than during cooling.

https://doi.org/10.1021/acs.nanolett.3c02260
Nano Lett. 2023, 23, 8801−8807

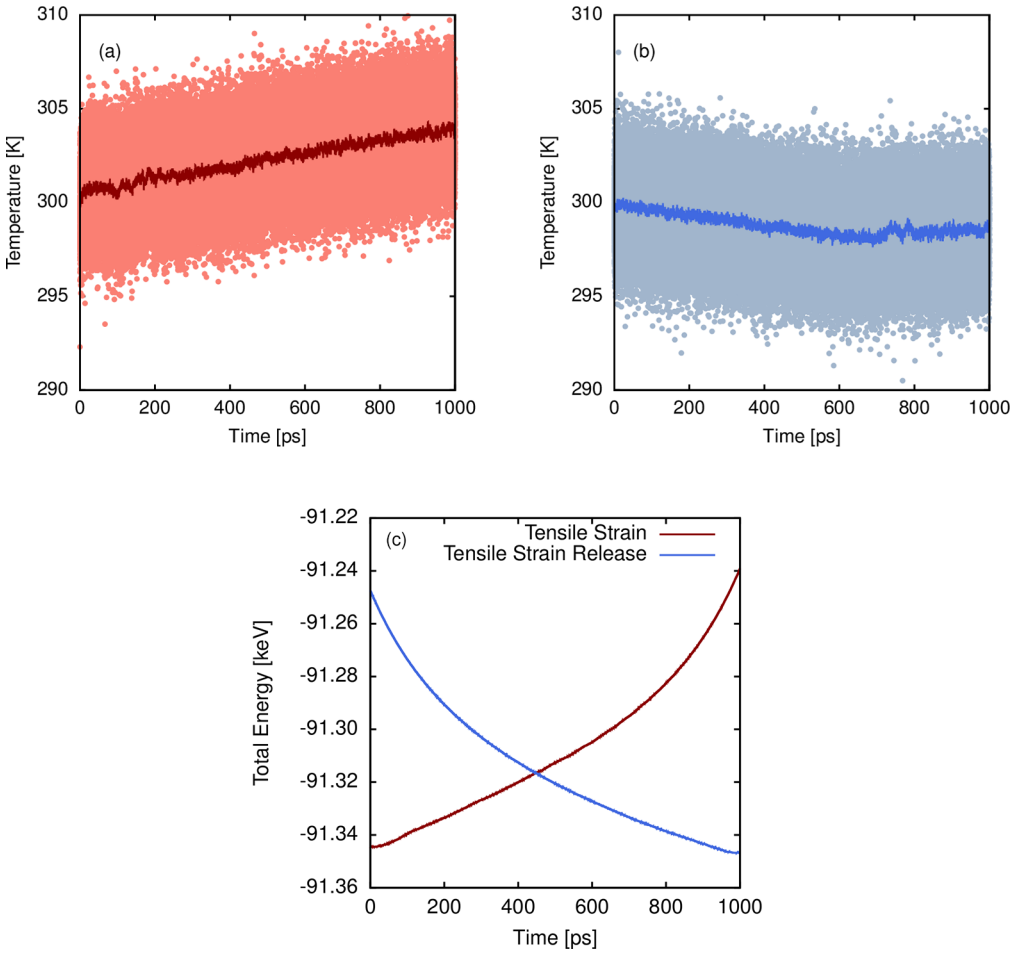

Figure 4. Time evolution of the GK temperature under (a) tensile stretching and (b) release for one particular seed. The red and blue lines are the moving averages for temperature calculated every 100 MD steps. Panel c illustrates the time evolution of total energy as a function of time. The red and blue curves refer to adiabatic tensile strain and the tensile strain release, respectively.

The GK coefficient-of-performance (COP) associated with heating or cooling can be calculated. To do that, we need to determine both the heat, Q, exchanged with a thermal bath and the work, W, done on and by the system during one full cycle. Processes 2 → 3 and 4 → 1 are isochoric and do not contribute to the total work per cycle, while processes 1 → 2 and 3 → 4 are adiabatic, meaning there is no heat exchange into or out of the GK monolayer. Therefore, the total energy change due to tensile or tensile release processes will equal the work done on or by the GK system.

The total energy values as a function of simulation time during the 1 → 2 tensile stretching process and the 3 → 4 releasing process are shown in Figure 4c, also just for one seed. W can then be calculated from these curves as the sum of variations in the internal energy of the GK during the processes 1 → 2 and 3 → 4, denoted $E_{1\to2}$ and $E_{3\to4}$, respectively. Specifically, their average values considering all seeds are $W = E_{1\to2} - E_{3\to4} = 109.5 - (-103.1) = 212.6$ eV.

To obtain the heat, Q, exchanged with the thermal bath, the thermal capacity, C, of GK was estimated using a series of equilibrium simulations at different temperature regimes, as shown in Figure 5. The thermalization of the GK over time and the relationship between the temperature of the system and its total energy are shown in Figure 5a and Figure 5b, respectively. Temperature values ranged from 50 to 1100 K in increments of 150 K.

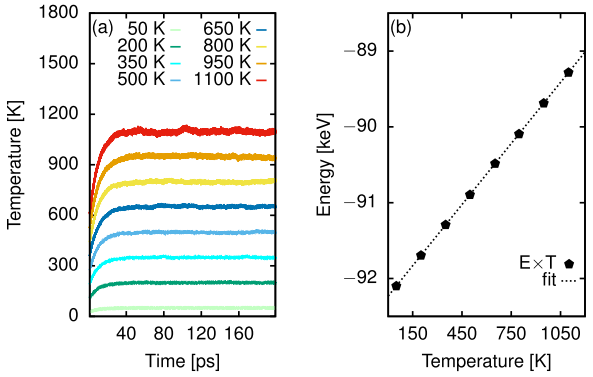

Figure 5. (a) Time evolution of the temperature (GK thermalization) and (b) total energy of the system as a function of its temperature. The temperature values used in these simulations vary from 50 K up to 1100 K with a step of 150 K.

Linear fitting of the data in Figure 5b resulted in a thermal capacity of $C_{MD} = \Delta E/\Delta T = 2.67$ eV/K; dividing by the mass of the GK and changing the units give the value mentioned previously of $c_{MD} = 1770$ J·kg^{-1}·K^{-1}. With c_{MD} and the values of ΔT_{MD}, one can calculate the heat transferred/extracted (Q_T/Q_E) to/from the thermal reservoir at 300 K: $Q_E = mc_{MD}\Delta T_{MD}$ and $Q_T = mc_{MD}\Delta T_{MD}$.

https://doi.org/10.1021/acs.nanolett.3c02260
Nano Lett. 2023, 23, 8801−8807

Finally, we calculate the COP for GK. Using the values derived above for Q and W, we obtain the COP for heat transfer and extraction (COP_T/COP_E) to/from the thermal reservoir: $COP_T = Q_T/W_{MD}$ and $COP_E = Q_E/W_{MD}$. Some alloys, for example, NiTi wires, show an ECE of about 17 K with a large COP of approximately 11.[74] Carbon nanotubes can exhibit an ECE varying between 40 K up to 100 K with also a large COP that ranges from 4 to 12.[58]

GK has reasonable temperature change values of approximately 9.32 K for heating and −3.50 K for cooling, as mentioned above, accompanied by equally reasonable COP values of approximately 1.57 and 0.62, respectively. Although these values are not as impressive as those of NiTi wires or carbon nanotubes, they represent about 23 and 8.8 times greater ECE temperature changes than those of macroscopic kirigami materials.[61] The Supporting Information provides the values for the aforementioned quantities for individual seeds, which were used to determine the COP.

In summary, our study investigated the ECE in a GK monolayer at the nanoscale, representing the thinnest possible KM. We compared the temperature changes of GK with macroscopic KMs, which was recently experimentally realized,[61] and identified key differences. Moreover, this study is the first to determine the COP in GK.

Through fully atomistic molecular dynamics simulations, we found that GK exhibited a relatively large temperature change of approximately 9.32 K for heating and −3.50 K for cooling. This temperature change is significantly higher than the changes observed in macroscopic KMs, which reached a maximum of approximately 0.4 K. The one-atom-thick configuration of graphene in GK prevented the complex temperature variations observed in macroscopic KMs, where simultaneous heating and cooling occurred in different regions when external strain was applied.

Our simulations also revealed that the deformation mechanism of GK involved elastic stretching of C−C bonds and out-of-plane buckling. The out-of-plane deflected regions did not experience cooling or warming, contrary to the behavior observed in macroscopic KMs. This disparity arose because the flexing of a one-atom-thick nanoribbon did not generate strain in the C−C bonds, unlike macroscopic kirigami structures.

We calculated the COP of GK, representing the ratio of heat transferred to/from the thermal reservoir to work performed on the system per thermodynamic cycle. Our results demonstrated a reasonable COP of approximately 1.57 (0.62) for GK as a solid heater (refrigerator), indicating its potential for heat transfer and extraction.

When the COP of GK is compared with that of other materials, such as alloys and carbon nanotubes, GK presents a smaller performance. However, neither alloys nor nanotubes can reversibly withstand a tensile strain as high as 30%. That feature might be considered when considering smart applications of GK as solid heaters or refrigerators at the nanoscale. Our findings highlight the unique behavior of GK at the nanoscale and its potential as a kirigami-based material for applications requiring substantial temperature changes and efficient heat transfer.

■ ASSOCIATED CONTENT

Supporting Information

The Supporting Information is available free of charge at https://pubs.acs.org/doi/10.1021/acs.nanolett.3c02260.

Calculated values for the quantities, including individual seed values and their corresponding averages, used to determine the COP; figures illustrating the thermodynamic cycles for simulations with 10 different seeds (PDF)

■ AUTHOR INFORMATION

Corresponding Author

Alexandre F. Fonseca − *Applied Physics Department, Gleb Wataghin Institute of Physics, University of Campinas, 13083-859 Campinas, São Paulo, Brazil;* orcid.org/0000-0001-8413-9744; Email: afonseca@ifi.unicamp.br

Authors

Luiz A. Ribeiro Junior − *Institute of Physics and Computational Materials Laboratory, LCCMat, Institute of Physics, University of Brasília, 70910-900 Brasília, Brazil*

Marcelo L. Pereira Junior − *Department of Electrical Engineering, Faculty of Technology, University of Brasília, 70910-900 Brasília, Brazil*

Complete contact information is available at: https://pubs.acs.org/10.1021/acs.nanolett.3c02260

Notes

The authors declare no competing financial interest.

■ ACKNOWLEDGMENTS

This work received partial support from Brazilian agencies CAPES, CNPq, and FAPDF. L.A.R.J. thanks the financial support from Brazilian Research Council FAP-DF Grants 00193-00000857/2021-14, 00193-00000853/2021-28, and 00193-00000811/2021-97, CNPq Grants 302236/2018-0 and 350176/2022-1, and FAPDF-PRONEM Grant 00193.00001247/2021-20. L.A.R.J. also thanks ABIN Grant 08/2019 and Núcleo de Computação de Alto Desempenho (NACAD) for computational facilities through the Lobo Carneiro supercomputer. A.F.F. is a Fellow of the Brazilian Agency CNPq-Brazil (Grant 303284/2021-8) and acknowledges Grant 2020/02044-9 from São Paulo Research Foundation (FAPESP). This work used resources of the Centro Nacional de Processamento de Alto Desempenho em São Paulo (CENAPAD-SP). The authors acknowledge the National Laboratory for Scientific Computing (LNCC/MCTI, Brazil) for providing HPC resources of the SDumont supercomputer, contributing to the research results reported within this paper: URL http://sdumont.lncc.br.

■ REFERENCES

(1) Geim, A. K. Graphene: status and prospects. *science* **2009**, *324*, 1530−1534.

(2) Novoselov, K. S.; Geim, A. K.; Morozov, S. V.; Jiang, D.-e.; Zhang, Y.; Dubonos, S. V.; Grigorieva, I. V.; Firsov, A. A. Electric field effect in atomically thin carbon films. *science* **2004**, *306*, 666−669.

(3) Papageorgiou, D. G.; Kinloch, I. A.; Young, R. J. Mechanical properties of graphene and graphene-based nanocomposites. *Prog. Mater. Sci.* **2017**, *90*, 75−127.

(4) Castro Neto, A. H.; Guinea, F.; Peres, N. M. R.; Novoselov, K. S.; Geim, A. K. The electronic properties of graphene. *Rev. Mod. Phys.* **2009**, *81*, 109.

(5) Bao, W.; Miao, F.; Chen, Z.; Zhang, H.; Jang, W.; Dames, C.; Lau, C. N. Controlled ripple texturing of suspended graphene and ultrathin graphite membranes. *Nat. Nanotechnol.* **2009**, *4*, 562.

(6) Xu, X.; Pereira, L. F. C.; Wang, Y.; Wu, J.; Zhang, K.; Zhao, X.; Bae, S.; Bui, C. T.; Xie, R.; Thong, J. T. L.; Hong, B. H.; Loh, K. P.;

Donadio, D.; Li, B.; Özyilmaz, B. Length-dependent thermal conductivity in suspended single-layer graphene. *Nat. Commun.* **2014**, *5*, 3689.
(7) Falkovsky, L. A. Optical properties of graphene. *Journal of Physics: conference series* **2008**, *129*, 012004.
(8) Lui, C. H.; Liu, L.; Mak, K. F.; Flynn, G. W.; Heinz, T. F. Ultraflat graphene. *Nature* **2009**, *462*, 339−341.
(9) Raccichini, R.; Varzi, A.; Passerini, S.; Scrosati, B. The role of graphene for electrochemical energy storage. *Nature materials* **2015**, *14*, 271−279.
(10) Chen, Y.; Tan, C.; Zhang, H.; Wang, L. Two-dimensional graphene analogues for biomedical applications. *Chem. Soc. Rev.* **2015**, *44*, 2681−2701.
(11) Akinwande, D.; Brennan, C. J.; Bunch, J. S.; Egberts, P.; Felts, J. R.; Gao, H.; Huang, R.; Kim, J.-S.; Li, T.; Li, Y.; et al. A review on mechanics and mechanical properties of 2D materials—Graphene and beyond. *Extreme Mechanics Letters* **2017**, *13*, 42−77.
(12) Blees, M. K.; Barnard, A. W.; Rose, P. A.; Roberts, S. P.; McGill, K. L.; Huang, P. Y.; Ruyack, A. R.; Kevek, J. W.; Kobrin, B.; Muller, D. A.; et al. Graphene kirigami. *Nature* **2015**, *524*, 204−207.
(13) Qi, Z.; Campbell, D. K.; Park, H. S. Atomistic simulations of tension-induced large deformation and stretchability in graphene kirigami. *Phys. Rev. B* **2014**, *90*, 245437.
(14) Hanakata, P. Z.; Cubuk, E. D.; Campbell, D. K.; Park, H. S. Accelerated search and design of stretchable graphene kirigami using machine learning. *Physical review letters* **2018**, *121*, 255304.
(15) Hua, Z.; Zhao, Y.; Dong, S.; Yu, P.; Liu, Y.; Wei, N.; Zhao, J. Large stretchability and failure mechanism of graphene kirigami under tension. *Soft Matter* **2017**, *13*, 8930−8939.
(16) Wei, N.; Chen, Y.; Cai, K.; Zhao, J.; Wang, H.-Q.; Zheng, J.-C. Thermal conductivity of graphene kirigami: Ultralow and strain robustness. *Carbon* **2016**, *104*, 203−213.
(17) Felix, L. C.; Tromer, R. M.; Autreto, P. A. S.; Ribeiro Junior, L. A.; Galvao, D. S. On the Mechanical Properties and Thermal Stability of a Recently Synthesized Monolayer Amorphous Carbon. *J. Phys. Chem. C* **2020**, *124*, 14855−14860.
(18) Grosso, B. F.; Mele, E. Bending rules in graphene kirigami. *Physical review letters* **2015**, *115*, 195501.
(19) Gao, Y.; Chen, W.; Liu, Y.; Wu, J.; Jing, H. Graphene kirigami as an ultra-permeable water desalination membrane. *Carbon* **2022**, *195*, 183−190.
(20) Mortazavi, B.; Lherbier, A.; Fan, Z.; Harju, A.; Rabczuk, T.; Charlier, J.-C. Thermal and electronic transport characteristics of highly stretchable graphene kirigami. *Nanoscale* **2017**, *9*, 16329−16341.
(21) Cai, K.; Luo, J.; Ling, Y.; Wan, J.; Qin, Q.-h. Effects of size and surface on the auxetic behaviour of monolayer graphene kirigami. *Sci. Rep.* **2016**, *6*, 35157.
(22) Yong, K.; De, S.; Hsieh, E. Y.; Leem, J.; Aluru, N. R.; Nam, S. Kirigami-inspired strain-insensitive sensors based on atomically-thin materials. *Mater. Today* **2020**, *34*, 58−65.
(23) Ning, X.; Wang, X.; Zhang, Y.; Yu, X.; Choi, D.; Zheng, N.; Kim, D. S.; Huang, Y.; Zhang, Y.; Rogers, J. A. Assembly of advanced materials into 3D functional structures by methods inspired by origami and kirigami: a review. *Advanced Materials Interfaces* **2018**, *5*, 1800284.
(24) Lee, H. C.; Hsieh, E. Y.; Yong, K.; Nam, S. Multiaxially-stretchable kirigami-patterned mesh design for graphene sensor devices. *Nano Research* **2020**, *13*, 1406−1412.
(25) Xu, K.; Lu, Y.; Honda, S.; Arie, T.; Akita, S.; Takei, K. Highly stable kirigami-structured stretchable strain sensors for perdurable wearable electronics. *Journal of Materials Chemistry C* **2019**, *7*, 9609−9617.
(26) Lundgren, C.; Kakanakova-Georgieva, A.; Gueorguiev, G. K. A perspective on thermal stability and mechanical properties of 2D Indium Bismide from ab initio molecular dynamics. *Nanotechnology* **2022**, *33*, 335706.
(27) Alves Machado Filho, M.; Hsiao, C.-L.; Dos Santos, R. B.; Hultman, L.; Birch, J.; Gueorguiev, G. K. Self-Induced Core−Shell InAlN Nanorods: Formation and Stability Unraveled by Ab Initio Simulations. *ACS Nanoscience Au* **2023**, *3*, 84−93.
(28) Sangiovanni, D. G.; Faccio, R.; Gueorguiev, G. K.; Kakanakova-Georgieva, A. Discovering atomistic pathways for supply of metal atoms from methyl-based precursors to graphene surface. *Phys. Chem. Chem. Phys.* **2022**, *25*, 829−837.
(29) Kolev, S.; Aleksandrov, H.; Atanasov, V.; Popov, V.; Milenov, T. Interaction of graphene with out-of-plane aromatic hydrocarbons. *J. Phys. Chem. C* **2019**, *123*, 21448−21456.
(30) Ratcliff, L. E.; Mohr, S.; Huhs, G.; Deutsch, T.; Masella, M.; Genovese, L. Challenges in large scale quantum mechanical calculations. *Wiley Interdiscip. Rev.: Comput. Mol. Sci.* **2017**, *7*, e1290.
(31) Farah, K.; Müller-Plathe, F.; Böhm, M. C. Classical reactive molecular dynamics implementations: State of the art. *ChemPhysChem* **2012**, *13*, 1127−1151.
(32) Senftle, T. P.; Hong, S.; Islam, M. M.; Kylasa, S. B.; Zheng, Y.; Shin, Y. K.; Junkermeier, C.; Engel-Herbert, R.; Janik, M. J.; Aktulga, H. M.; et al. The ReaxFF reactive force-field: development, applications and future directions. *npj Comput. Mater.* **2016**, *2*, 1−14.
(33) Brenner, D. W.; Shenderova, O. A.; Harrison, J. A.; Stuart, S. J.; Ni, B.; Sinnott, S. B. A second-generation reactive empirical bond order (REBO) potential energy expression for hydrocarbons. *J. Phys.: Condens. Matter* **2002**, *14*, 783.
(34) Liang, T.; Shan, T.-R.; Cheng, Y.-T.; Devine, B. D.; Noordhoek, M.; Li, Y.; Lu, Z.; Phillpot, S. R.; Sinnott, S. B. Classical atomistic simulations of surfaces and heterogeneous interfaces with the charge-optimized many body (COMB) potentials. *Materials Science and Engineering: R: Reports* **2013**, *74*, 255−279.
(35) Gao, Y.; Lu, S.; Chen, W.; Zhang, Z.; Gong, C. Study on the Shear Behaviour and Fracture Characteristic of Graphene Kirigami Membranes via Molecular Dynamics Simulation. *Membranes* **2022**, *12*, 886.
(36) Li, H.; Cheng, G.; Liu, Y.; Zhong, D. Anomalous thermal response of graphene kirigami induced by tailored shape to uniaxial tensile strain: a molecular dynamics study. *Nanomaterials* **2020**, *10*, 126.
(37) Gamil, M.; Pei, Q.; Zhang, Y. Mechanical behaviour of kirigami graphene under shear loading. *Comput. Mater. Sci.* **2020**, *173*, 109462.
(38) Jang, H.; Park, Y. J.; Chen, X.; Das, T.; Kim, M.-S.; Ahn, J.-H. Graphene-based flexible and stretchable electronics. *Adv. Mater.* **2016**, *28*, 4184−4202.
(39) Hanakata, P. Z.; Qi, Z.; Campbell, D. K.; Park, H. S. Highly stretchable MoS 2 kirigami. *Nanoscale* **2016**, *8*, 458−463.
(40) Wang, B.; Nakano, A.; Vashishta, P. D.; Kalia, R. K. Nanoindentation on monolayer MoS2 kirigami. *ACS omega* **2019**, *4*, 9952−9956.
(41) Han, T.; Scarpa, F.; Allan, N. L. Super stretchable hexagonal boron nitride Kirigami. *Thin Solid Films* **2017**, *632*, 35−43.
(42) Mañosa, L.; Planes, A.; Acet, M. Advanced materials for solid-state refrigeration. *J. Mater. Chem. A* **2013**, *1*, 4925−4936.
(43) Moya, X.; Kar-Narayan, S.; Mathur, N. D. Caloric materials near ferroic phase transitions. *Nat. Mater.* **2014**, *13*, 439−450.
(44) Moya, X.; Mathur, N. D. Caloric materials for cooling and heating. *Science* **2020**, *370*, 797−803.
(45) Chauhan, A.; Patel, S.; Vaish, R.; Bowen, C. R. A review and analysis of the elasto-caloric effect for solidstate refrigeration devices: Challenges and opportunities. *MRS Energy Sustainability* **2015**, *2*, 16.
(46) Schmidt, M.; Schütze, A.; Seelecke, S. Elastocaloric cooling processes: The influence of material strain and strain rate on efficiency and temperature span. *APL Materials* **2016**, *4*, 064107.
(47) Tušek, J.; Engelbrecht, K.; Eriksen, D.; Dall'Olio, S.; Tušek, J.; Pryds, N. A regenerative elastocaloric heat pump. *Nature Energy* **2016**, *1*, 16134.
(48) Cazorla, C.; Errandonea, D. Giant Mechanocaloric Effects in Fluorite-Structured Superionic Materials. *Nano Lett.* **2016**, *16*, 3124−3129.
(49) Wang, R.; et al. Torsional refrigeration by twisted, coiled, and supercoiled fibers. *Science* **2019**, *366*, 216−221.

https://doi.org/10.1021/acs.nanolett.3c02260
Nano Lett. 2023, 23, 8801−8807

(50) Miliante, C. M.; Christmann, A. M.; Usuda, E. O.; Imamura, W.; Paixão, L. S.; Carvalho, A. M. G.; Muniz, A. R. Unveiling the Origin of the Giant Barocaloric Effect in Natural Rubber. *Macromolecules* **2020**, *53*, 2606−2615.
(51) Imran, M.; Zhang, X. Reduced dimensions elastocaloric materials: A route towards miniaturized refrigeration. *Materials & Design* **2021**, *206*, 109784.
(52) Lisenkov, S.; Herchig, R.; Patel, S.; Vaish, R.; Cuozzo, J.; Ponomareva, I. Elastocaloric effect in carbon nanotubes and graphene. *Nano Lett.* **2016**, *16*, 7008−7012.
(53) Zhang, J. Elastocaloric effect on the piezoelectric potential of boron nitride nanotubes. *J. Phys. D: Appl. Phys.* **2017**, *50*, 415308.
(54) Skačej, G. Elastocaloric effect in liquid crystal elastomers from molecular simulations. *Liq. Cryst.* **2018**, *45*, 1964−1969.
(55) Cantuario, T. E.; Fonseca, A. F. High Performance of Carbon Nanotube Refrigerators. *Annalen Der Physik* **2019**, *531*, 1800502.
(56) Warzoha, R. J.; Vu, N. T.; Donovan, B. F.; Cimpoiasu, E.; Sharar, D. J.; Leff, A. C.; Wilson, A. A.; Smith, A. N. Grain growth-induced thermal property enhancement of NiTi shape memory alloys for elastocaloric refrigeration and thermal energy storage systems. *Int. J. Heat Mass Transfer* **2020**, *154*, 119760.
(57) Li, M.; Guo, Z.; Chang, T. Adhesion and stress-enhanced elastocaloric effect in graphene. *Science China Technological Sciences* **2020**, *63*, 297−302.
(58) Silva, T. N. Y.; Fonseca, A. F. High performance of carbon nanotube elastocaloric refrigerators over a large temperature span. *Phys. Rev. B* **2022**, *106*, 165413.
(59) Liu, J.; He, J.; Ma, S. Large Elastocaloric Effect Driven by Low Stress Induced in [001]-Oriented Polycrystalline Co51. 6V31. 4Ga17 Alloy. *Magnetochemistry* **2022**, *8*, 87.
(60) Zhao, Z.; Guo, W.; Zhang, Z. Room-Temperature Colossal Elastocaloric Effects in Three-Dimensional Graphene Architectures: An Atomistic Study. *Adv. Funct. Mater.* **2022**, *32*, 2203866.
(61) Hirai, T.; Iguchi, R.; Miura, A.; Uchida, K.-i. Elastocaloric Kirigami Temperature Modulator. *Adv. Funct. Mater.* **2022**, *32*, 2201116.
(62) Thompson, A. P.; Aktulga, H. M.; Berger, R.; Bolintineanu, D. S.; Brown, W. M.; Crozier, P. S.; in't Veld, P. J.; Kohlmeyer, A.; Moore, S. G.; Nguyen, T. D.; et al. LAMMPS-a flexible simulation tool for particle-based materials modeling at the atomic, meso, and continuum scales. *Comput. Phys. Commun.* **2022**, *271*, 108171.
(63) Stuart, S. J.; Tutein, A. B.; Harrison, J. A. A reactive potential for hydrocarbons with intermolecular interactions. *J. Chem. Phys.* **2000**, *112*, 6472−6486.
(64) Grantab, R.; Shenoy, V. B.; Ruoff, R. S. Anomalous strength characteristics of tilt grain boundaries in graphene. *Science* **2010**, *330*, 946.
(65) Neek-Amal, M.; Peeters, F. M. Lattice thermal properties of graphane: Thermal contraction, roughness, and heat capacity. *Phys. Rev. B* **2011**, *83*, 235437.
(66) Gao, W.; Huang, R. Thermomechanics of monolayer graphene: Rippling, thermal expansion and elasticity. *Journal of the Mechanics and Physics of Solids* **2014**, *66*, 42.
(67) Mostério, N. C. B.; Fonseca, A. F. Thermal expansion behavior of holes in graphene nanomeshes. *Phys. Rev. B* **2014**, *89*, 195437.
(68) Muniz, A. R.; Fonseca, A. F. Carbon-Based Nanostructures Derived from Bilayer Graphene with Zero Thermal Expansion Behavior. *J. Phys. Chem. C* **2015**, *119*, 17458−17465.
(69) Li, Q.-Y.; Xia, K.; Zhang, J.; Zhang, Y.; Li, Q.; Takahashi, K.; Zhang, X. Measurement of specific heat and thermal conductivity of supported and suspended graphene by a comprehensive Raman optothermal method. *Nanoscale* **2017**, *9*, 10784−10793.
(70) Bu, H.; Chen, Y.; Zou, M.; Yi, H.; Bi, K.; Ni, Z. Atomistic simulations of mechanical properties of graphene nanoribbons. *Phys. Lett. A* **2009**, *373*, 3359−3362.
(71) Ni, Z.; Bu, H.; Zou, M.; Yi, H.; Bi, K.; Chen, Y. Anisotropic mechanical properties of graphene sheets from molecular dynamics. *Physica B: Condensed Matter* **2010**, *405*, 1301−1306.
(72) Pei, Q.; Zhang, Y.; Shenoy, V. A molecular dynamics study of the mechanical properties of hydrogen functionalized graphene. *Carbon* **2010**, *48*, 898−904.
(73) Zhang, D. B.; Akatyeva, E.; Dumitrică, T. Bending Ultrathin Graphene at the Margins of Continuum Mechanics. *Phys. Rev. Lett.* **2011**, *106*, 255503.
(74) Cui, J.; Wu, Y.; Muehlbauer, J.; Hwang, Y.; Radermacher, R.; Fackler, S.; Wuttig, M.; Takeuchi, I. Demonstration of high efficiency elastocaloric cooling with large ΔT using NiTi wires. *Appl. Phys. Lett.* **2012**, *101*, 073904.

https://doi.org/10.1021/acs.nanolett.3c02260
Nano Lett. 2023, 23, 8801−8807